ACS APPLIED MATERIALS & INTERFACES

Research Article

www.acsami.org

Harnessing Phosphato-Platinum Bonding Induced Supramolecular Assembly for Systemic Cisplatin Delivery

Yingqin Hou,[†,∥] Yaoyi Wang,[†,∥] Ruijue Wang,[§] Weier Bao,[‡] Xiaobo Xi,[‡] Yunlong Sun,[†] Shengtao Yang,[§] Wei Wei,[*,‡] and Hua Lu[*,†]

[†]Beijing National Laboratory for Molecular Sciences, Center for Soft Matter Science and Engineering, Key Laboratory of Polymer Chemistry and Physics of Ministry of Education, College of Chemistry and Molecular Engineering, Peking University, Beijing 100871, People's Republic of China

[‡]State Key Laboratory of Biochemical Engineering, Institute of Process Engineering, Chinese Academy of Sciences, Beijing 10090, People's Republic of China

[§]College of Chemistry and Environment Protection Engineering, Southwest University for Nationalities, Chengdu 610041, People's Republic of China

Supporting Information

ABSTRACT: To improve the therapeutic index of cisplatin (CDDP), we present here a new paradigm of drug-induced self-assembly by harnessing phosphato-platinum complexation. Specifically, we show that a phosphato-platinum cross-linked micelle (PpY/Pt) can be generated by using a block copolymer methoxy-poly(ethylene glycol)-*block*-poly(L-phosphotyrosine) (mPEG-*b*-PpY). Coating of PpY/Pt with a R_9-iRGD peptide by simple mixing affords a targeting micelle with near neutral-charged surface (iPpY/Pt). The micelles feature in well-controlled sizes below 50 nm and high stability under physiological conditions, and can withstand various environmental stresses. Importantly, the micelles demonstrate on-demand drug release profiles in response to pathological cues such as high ATP concentration and acidic pH. In vitro, the micelles are efficiently internalized and almost equally potent compared to CDDP. Moreover, iPpY/Pt induce greater cytotoxicity than PpY/Pt in a 3D tumor spheroid model likely due to its deeper tumor penetration. In vivo, the micelles exhibit prolonged circulation half-lives, enhanced tumor accumulation, excellent tumor growth inhibition in a xenograft HeLa model and an orthotropic mammary 4T1 model, and improved safety profiles evidenced by the reduced nephrotoxicity. Together, this work demonstrates for the first time that phosphato-platinum complexation can be exploited for effective delivery of CDDP, and suggests a paradigm shift of constructing nanosystems for other anticancer metallodrugs.

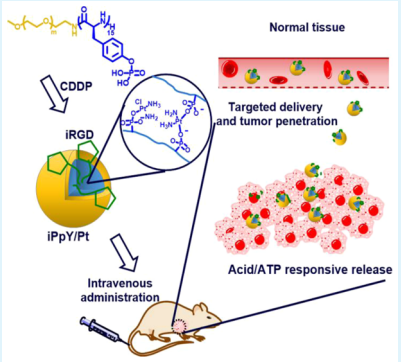

KEYWORDS: *poly(phosphotyrosine), cisplatin, ATP-responsive, drug delivery, iRGD*

1. INTRODUCTION

cis-Diamminedichloridoplatinum(II) (CDDP), also known as cisplatin, is a widely used first-line chemotherapy agent for various cancers including lymphoma, bladder, testis, and ovarian cancer.[1] However, CDDP suffers rapid clearance from the plasma, unsatisfactory efficacy, and severe systemic toxicity, primarily nephrotoxicity. As such, the clinical use of cisplatin is dose-limited. To improve the therapeutic index of CDDP, Pt(II), or Pt(IV) (pro)drugs[2] with additional mechanisms such as HSA-binding,[3,4] targeting,[5] anti-inflammation,[6] and immunotherapy have been broadly explored.[7] Another approach capitalizes on various delivery systems[8,9] in which the platinum-based drugs, sometimes together with siRNAs[10−14] or other chemotherapeutics,[15−20] were encapsulated or conjugated to carriers such as inorganic particles,[21−26] metal−organic frameworks (MOFs),[27,28] lipid based nanoparticles,[29−31] and polymeric nanoparticles.[32−43]

Cisplatin is known to be rapidly hydrated to generate the highly reactive *cis*-$[Pt(NH_3)_2(H_2O)_2]^{2+}$, which ultimately leads to its potency and toxicity. Substantial efforts, therefore, have been focusing on modifying the leaving group attached to platinum to fine-tune the hydration rate. Among these strategies, carboxylato-platinum bonding is currently the most prevailing approach to formulating CDDP-based nanomedicine.[19,20,39,40,44−46] For instance, carboxylato-platinum cross-linked polyethylene glycol-*block*-poly(L-glutamate) (PEG-*b*-PLG) micelles have advanced to different stages of clinical trials and hold considerable promise for translating the system from bench to bedside.[47,48] Nevertheless, this strategy often yields hampered drug internalization and significant loss (sometimes ~90%) of anticancer activity in vitro.[35,49] In this regard, further optimization of the potency and other related pharmacological characters of CDDP through engineering the

Received: March 15, 2017
Accepted: May 8, 2017
Published: May 8, 2017

DOI: 10.1021/acsami.7b03686
ACS Appl. Mater. Interfaces 2017, 9, 17757−17768

platinum complexation environment is of utmost importance.[50−52]

To improve the effectiveness of cisplatin delivery systems, here we aim to interrogate the drug-induced self-assembly by harnessing a relatively less-explored phosphato-platinum bond.[53] For this, we rationalize that a block copolymer methoxy-poly(ethylene glycol)-*block*-poly(L-phosphotyrosine) (mPEG-*b*-PpY) can serve as an excellent carrier. PpY is a bioinspired and biodegradable poly(α-amino acid) mimicking tyrosine phosphorylation, a vital post-translational modification.[54,55] We expect that the peptidic hydrogen bonding[48] and side-chain $\pi-\pi$ interaction of PpY may generate additional interactions to stabilize the nanomedicine during circulation. Interestingly, besides the conceivable acid-triggered drug release, we unexpectedly observe a rapid and profound ATP-induced platinum release, suggesting a multilayered mechanism of action for selective and intracellular delivery of this novel nanosystem.

2. EXPERIMENTAL SECTION

2.1. Materials. All chemicals were purchased from commercial sources and used as received unless otherwise specified. Anhydrous *N*,*N*-dimethylformamide (DMF) was purchased from Sigma-Aldrich (St. Louis, U.S.A.) and treated with methyl isocyanate bounded polystyrene beads (Sigma-Aldrich, St. Louis, U.S.A.) prior to polymerization. Dry $CDCl_3$ was prepared by treating commercial $CDCl_3$ with $CaSO_4$ overnight. pOEt-TyrNCA was synthesized following previously reported procedure.[55] mPEG-NH_2 (M_W = 5000) was purchased from Aladdin Bio-Chem Technology Co. Ltd. (Shanghai, China). Cy5 NHS ester was purchased from Okeanos Tech. Co. Ltd. (Beijing, China). Peptide R_9-iRGD (R_9G_2C**RGD**RGPDC, underline denotes disulfide bond) and R_9-iKGD (R_9G_2C**KGD**RGPDC, underline denotes disulfide bond) were synthesized by standard Fmoc solid phase peptide synthesis (SPPS) on a CS Bio peptide synthesizer CS136S (CS Bio Co.) and purified using reverse phase High Performance Liquid Chromatography (RP-HPLC, LC20A, Shimazu, Japan).

2.2. Instruments. NMR Spectra were recorded on a Bruker-400 MHz NMR spectrometer (ARX 400, Bruker Co., Germany). Ultraperformance liquid chromatography electrospray ionization mass spectrometry (UPLC-ESIMS) analyses were performed on a system equipped with an ACQUITY H-Class UPLC (Waters Corp. U.S.A) and a quadrupole rods SQ Detector 2 mass spectrometer (Waters Corp. U.S.A). For peptide analysis, separations were realized by a peptide BEH C18 column (Waters 300 Å, 1.7 μm; 2.1 × 100 mm^2) using ultrapure water plus 0.1% formic acid and acetonitrile as the mobile phase. Tandem gel permeation chromatography (GPC) experiments were performed on a system equipped with an isocratic pump (Model 1100, Agilent Technology, Santa Clara, CA), a DAWN HELEOS 9-angle laser light scattering detector (Wyatt Technology, Santa Barbara, CA) and an Optilab rEX refractive index detector (Wyatt Technology, Santa Barbara, CA). The detection wavelength of HELEOS was set at 658 nm. Separations were performed using serially connected size exclusion columns (500 Å, 10^3 Å, 10^4 Å Phenogel columns, 5 μm, 7.8 × 300 mm^2, Phenomenex, Torrance, CA) at 50 °C using DMF containing 0.1 M LiBr as the mobile phase. The molecular weight (M_W) of mPEG-P(pOEt-Tyr)$_{15}$ was calculated based on the dn/dc values previously reported.[55] Dynamic light scattering and zeta potential were measured on a Nanobrook Omni (Brookhaven Instrument Corp. at 25 °C (New York, U.S.A.). ICP Mass Spectrometry (ICP-MS) were performed on a NexION 350X (PerkinElmer, U.S.A). Transmission electron microscopy (TEM) experiments were performed on a JEM-2100F microscope (JEOL Ltd., Japan). CLSM images were taken on a Nikon A1R confocal laser scanning microscope system attached to an inverted ECLIPSE Ti (Nikon Corp. Japan). Circular Dichroism (CD) spectroscopy was recorded on a MOS-500 CD Spectrometer (Bio-Logic Science Instruments, France) with a 0.1 cm path length quartz cell. Cytotoxicity studies were assayed with an EnSpire Multimode Plate Reader (PerkinElmer, U.S.A.). Microvolume UV−vis (nanodrop) measurements were recorded on a NanoPhotometer P-Class (Implen, Germany). Flow cytometry analysis was performed on a BD LSR Fortessa equipped with 405, 488, and 640 nm lasers (BD Bioscience. U.S.A.). Blood biochemical analysis was recorded by Toshiba Accute Biochemical (Analyzer TBA-40FR). The histologic section was imaging on a Laser scanning quantitative imaging system (Vectra).

2.3. Cells and Animals. Human cervical cancer cell line HeLa, human liver hepatocellular carcinoma cell line HepG2, human osteosarcoma cell line Saos-2 (Sarcoma osteogenic) and U-2 OS were grown in DMEM (Corning, Manassas, U.S.A.) supplemented with 10% FBS, 100 U mL^{-1} of penicillin and 100 U mL^{-1} of streptomycin. Mouse breast cancer cell line 4T1 and human ovarian carcinoma cell line SKOV3 were maintained in RPMI 1640 (Corning, Manassas, U.S.A.) supplemented with 10% FBS, 100 U mL^{-1} of penicillin and 100 U mL^{-1} of streptomycin. The cells were incubated in a humidified incubator with 5% CO_2 at 37 °C. Six-week old female BALB/c mice were ordered from Vital River Laboratories (Beijing, China). All animal experiments were performed in compliance with the guide for the Care and Use of Laboratory Animals, and were approved by the Experimental Animal Ethics Committee in Beijing.

2.4. Synthesis of mPEG-*b*-PpY. As shown in Scheme S1, in a glovebox, pOEt-TyrNCA (104.1 mg, 15.0 equiv) was dissolved in anhydrous DMF (200 μL), to which was added mPEG-NH_2 (107.7 mg, 1.0 equiv) in DMF (500 μL) under stirring. The polymerization mixture was stirred at room temperature for 48 h when pOEt-TyrNCA was completely consumed. The product mPEG-P(pOEt-Tyr)$_{15}$ was precipitated in diethyl ether (20.0 mL) and washed with diethyl ether (20.0 mL × 4) to afford a white powder with a ~64% yield. mPEG-P(pOEt-Tyr)$_{15}$ was characterized by GPC and ^{1}H NMR spectroscopy before deprotection.

To syntehsize mPEG-*b*-PpY, bromotrimethysilane (TMSBr, 600 μL, 4.5 mmol) and triethylamine (TEA, 500 μL, 3.5 mmol) were added to mPEG-P(pOEt-Tyr)$_{15}$ (~128−135 mg) in DCM (1.0 mL) under stirring at room temperature. The mixture was continuously stirred at 60 °C for 10 h before it was concentrated under vacuum. The crude product was dissolved in water and purified by dialysis against 100 mM NaCl for 4 h, followed by dialysis against ultrapure water for another 8 h (water changed every 2 h). The resulting light yellow solution was lyophilized to afford mPEG-*b*-PpY as a brown powder (yield ~60%). The product was confirmed by ^{1}H NMR spectroscopy.

2.5. Cy5 NHS Labeling. mPEG-*b*-PpY (30 mg) was dissolved in dry methanol (2.0 mL), to which was added Cy5 NHS ester (2 wt %) and triethylamine (50 μL). After incubation at room temperature for 24 h, the solution was ultrafiltrated (MWCO 3000) at 2850 *g* repetitively to remove the excess dye until the fluorescence intensity of the flow-through plunged down to ~1% of the polymer solution on top. The purified Cy5 labeled mPEG-*b*-PpY was lyophilized to afford a brown powder in ~55% yield.

2.6. Preparation of PpY/Pt. Cisplatin (8.0 mg, 1.0 equiv) and $AgNO_3$ (8.2 mg, 1.9 equiv) were vigorously stirred in H_2O (1.0 mL) at room temperature in dark for 12 h. The suspension was centrifuged at 13800 *g* for 15 min and the supernatant was filtered by a 0.22 μm filter to afford an aqueous solution of *cis*-$[Pt(NH_3)_2(H_2O)_2](NO_3)_2$, which was added dropwise to mPEG-*b*-PpY (7.6 mg) in H_2O (2.0 mL) at a feeding molar ratio P/Pt = 2/1. The reaction was stirred at 1200 rpm and room temperature for 14 h to yield a light blue solution. PpY/Pt was then purified and concentrated by ultrafiltration for three times (4000 *g* × 20 min); iPpY/Pt was obtained by mixing PpY/Pt and iRGD at a feeding polymer/peptide molar ratio of 5:3 and used without further purification. The contents of Pt and P in the nanoparticles were determined by ICP-MS. Drug loading content (DLC) and drug loading efficiency (DLE) were calculated according to the following formula:

$$\text{DLC (wt\%)} = (\text{weight of drug loaded/weight of nanoparticle}) \times 100\%$$

DOI: 10.1021/acsami.7b03686
ACS Appl. Mater. Interfaces 2017, 9, 17757−17768

$$\text{DLE}\ (\%) = (\text{mol of Pt loaded/mol of Pt fed}) \times 100\%$$

Fluorescent dye labeled PpY/Pt and iPpY/Pt was prepared via a similar protocol by using Cy-5 labled mPEG-*b*-PpY.

2.7. Transmission Electron Microscope (TEM). All samples were diluted in Na_2SO_4 (50 μM × 990 μL) to give nanoparticle solutions at 0.1 mg/mL. Typically, an aliquot (10 μL) of the solution was deposited onto a 200-mesh copper grid coated with carbon, and was allowed to dry at room temperature with the help of a filter paper absorbing water from the other side of the grid. Transmission electron micrographs of the nanoparticles were analyzed with a transmission electron microscope (JEM-2100F, Japan) equipped with a field emission gun, ultrahigh-resolution pole piece, and ultrathin window JEOL detector at an accelerating voltage of 200 kV. Images were obtained with an OSIS CANTEGA CCD camera.

2.8. Release Kinetics. The release kinetics of PpY/Pt and iPpY/Pt was measured in a similar way. Briefly, for example, a PpY/Pt solution (500 μL, 698 μg Pt) was dispersed in DMEM (500 μL) to make a final volume of 1000 μL. The solution was placed into a dialysis bag (MWCO 1000 Da) and incubated in DMEM medium plus 10% FBS (99.0 mL) at 37 °C. At each time point, 1.0 mL solution outside the dialysis bag was taken out and sampled for Pt concentration by ICP-MS. In order to keep the total volume unchanged outside the dialysis bag, 1.0 mL fresh DMEM medium plus 10%FBS was supplied back to the solution each time.

The release kinetics of PpY/Pt at different pHs were measured by following a similar protocol except that the dialysis buffer was changed to PBS. The release kinetics of PpY/Pt (0.1 mM Pt in 100 μL 1 × PBS) in the presence 10 mM ATP, GTP, CTP or UTP were performed in a Tube-O-dialyzer (MWCO 1000) at 37 °C. All experiments were repeated in duplicates.

2.9. CD Analysis. All samples (0.1 mg/mL of nanoparticle) in PBS (pH 7.5) were degassed by N_2 for 10 min before measurement in a quartz cell (0.1 cm path length). CD spectra were recorded on a CD spectrometer (Bio-Logic Science Instruments, France; wavelength: 190−250 nm; scan rate: 100 nm/min; bandwidth: 1 nm; scan point interval: 1.0 nm; temperature: 37 °C). The molar ellipticity was calculated following equation: $[\theta]$ (deg·cm^2·dmol^{-1}) = (millidegrees × mean residue weight in mg/mL)/(path length in millimeters × concentration of polypeptide in mg/mL).

2.10. Cell Viability Assay. Cells were seeded in a 96-well plate at a density of 5000 cells per well (for 48 h-assay) or 3000 cells per well (for 72 and 96 h assays) 24 h prior to treatment. The cells were incubated with CDDP or micelles at gradient concentrations for 48 h (n = 3), 72 or 96 h (n = 5). Cell viabilities were determined by either CellTiter-Blue Cell Viability Assay (Promega, U.S.A.) for HepG-2, Saos-2 and SKOV3 cells, or 3-(4,5)-dimethylthiahiazo(-z-yl)-3,5-diphenyltetrazoliumromide (MTT) assay for all other cell lines. Both assays were performed by following manufacturers' procedures. IC_{50} values were obtained from GraphPad Prism version5.

2.11. Cell Uptake Analyzed by Flow Cytometry. Cells (1.0 × 10^5/well) were seeded in a 12-well plate and incubated for 24 h at 37 °C. Fresh medium containing Cy5-PpY/Pt or Cy5-iPpY/Pt (30 or 50 μM) was then supplemented to the cells. After 4 h incubation, cells were washed sequentially with PBS buffer (1.0 mL × 2), poly(D-lysine) (1.0 mg/mL, 1.0 mL), and PBS buffer (1.0 mL × 2). The cells were then digested by 0.05% trypsin, centrifuged, and resuspended in PBS for flow cytometry analysis.

2.12. Quantification of Platinum in Cell Lysates and Genomic DNA. Cells (5 × 10^6) were seeded in Corning 100 mm TC-Treated Culture Dishes 24 h prior to experiments. The cells were treated with CDDP or micelles at designated concentrations (10, 30, or 50 μM platinum) for varied incubation durations (4−36 h). The cells were washed with cold PBS (5.0 mL × 2), trypsinized, suspended in cold PBS (5.0 mL), and then centrifuged (800 g × 4 min at 4 °C) to afford cell pellets. After another two cycles of washing and centrifugation, the final pellets were resuspended in PBS (1.0 mL) and cell numbers were counted. The suspension was evenly divided into two groups: half of the cells were digested directly with concentrated MOS nitric acid (3.0 mL) for cellular Pt uptaking analysis, and the other half was used for genomic DNA platination analysis. Genomic DNA of HeLa cells was isolated by using a Wizard Genomic DNA Purification Kit (Promega, USA) and quantified on a NanoPhotometer P-Class (Implen, Germany). Quantification of Pt content in both cell lysates and genomic DNAs was measured by ICP-MS.

For platinum uptaking study in sodium azide treated cells, the cells were incubated with sodium azide (10 mM) 1 h before CDDP or micelles was implemented. All the experiments were performed in triplicate.

2.13. Penetration and Growth Inhibition of PpY/Pt and iPpY/Pt on MCTSs. MCTSs of 4T1 were prepared by following a reported method.[56] To evaluate the penetration of drugs, MCTSs were incubated with Cy5-PpY/Pt or Cy5-iPpY/Pt (30 μM platinum) for 72 h and analyzed by CLSM. To estimate the growth inhibition effect of PpY/Pt and iPpY/Pt on MCTSs, the 4T1 MCTSs were incubated with CDDP, PpY/Pt, or iPpY/Pt (50 μM) and growth inhibition of the tumor spheroid was monitored by an inverted phase microscope every 48 h.

2.14. Plasma Clearance and Tumor accumulation. BALB/c mice (n = 5) bearing 4T1 tumor model were treated with CDDP or micelles at a 100 μg/mouse dose (based on CDDP). Mice were sacrificed at each determined time point to collect the tumor and blood. The blood was treated with heparin for anticlotting and centrifuged to obtain plasma for Pt analysis. The tumors were washed with cold PBS and weighted after removal of excess fluid. All samples were completely digested by MOS nitric acid and evaporated to dryness. The platinum concentration was measured by ICP-MS after redissolving the samples in water. The plasma half-life of the samples was determined by the following equation:

$$\text{plasma half-life} = 0.693 \times T_{\text{interval}}/[\ln(C_{\text{peak}}) - \ln(C_{\text{trough}})]$$

where T_{interval} is the time between the peak and the lowest point, C_{peak} is the maximum concentration in plasma, and C_{trough} is the concentration at the end point. The statistical significance of different findings between the groups was determined by two-way ANOVA ananlysis. The results were considered statistically significant if the two-tailed P values were less than 0.05.

2.15. In Vivo Tumor Growth Inhibition. The human cervical carcinoma HeLa xenograft tumor model was established by subcutaneous injection of HeLa cells (6.0 × 10^6 in 100 μL PBS) into the right flank of each BALB/c-nu mouse. When the tumor reached ∼50 mm^3 (∼14 days after tumor inoculation), the mice was randomized into 4 groups (n = 5). PBS, CDDP, PpY/Pt, or iPpY/Pt therapy was administrated to the mice at a 1.5 mg/kg platinum dose once every other day via tail-vein injection. The tumor size and body weight of the mice were recorded once every other day.

The orthotopic mammary model of 4T1 tumor was established by subcutaneous injection of 4T1 cells (1.0 × 10^6 in 100 μL PBS) into the right flank of each BALB/c mouse. When the tumor reached ∼50 mm^3 (∼7 days after tumor inoculation), the mice was randomly grouped (n = 10). PBS, CDDP, PpY/Pt, or iPpY/Pt therapy was administrated to the mice at a 3.0 mg/kg platinum dose once every other day via tail-vein injection. The tumor size and body weight were recorded once every other day.

Tumor volume was calculated by the following formula:

$$V = L \times W^2/2$$

Relative tumor volume was calculated by the formula: $R = V/V_0$, where V_0 is the average tumor volume on day 0 (the start date of therapy). The relative body weight (R) was calculated by the formula: $R = W/W_0$, where W_0 is the body weight before administration.

2.16. Histopathology Evaluation. The histopathology damage evaluation was assessed by hematoxylin and eosin (H-E) method. Briefly, tumor, liver, kidney, heart, lung, and spleen were dissected, embedded with paraffin and cut into 5 μm thickness. The tissues were stained with H-E by a standard protocol to assess histopathology alterations by using laser scanning quantitative imaging system (Vectra).

DOI: 10.1021/acsami.7b03686
ACS Appl. Mater. Interfaces 2017, 9, 17757−17768

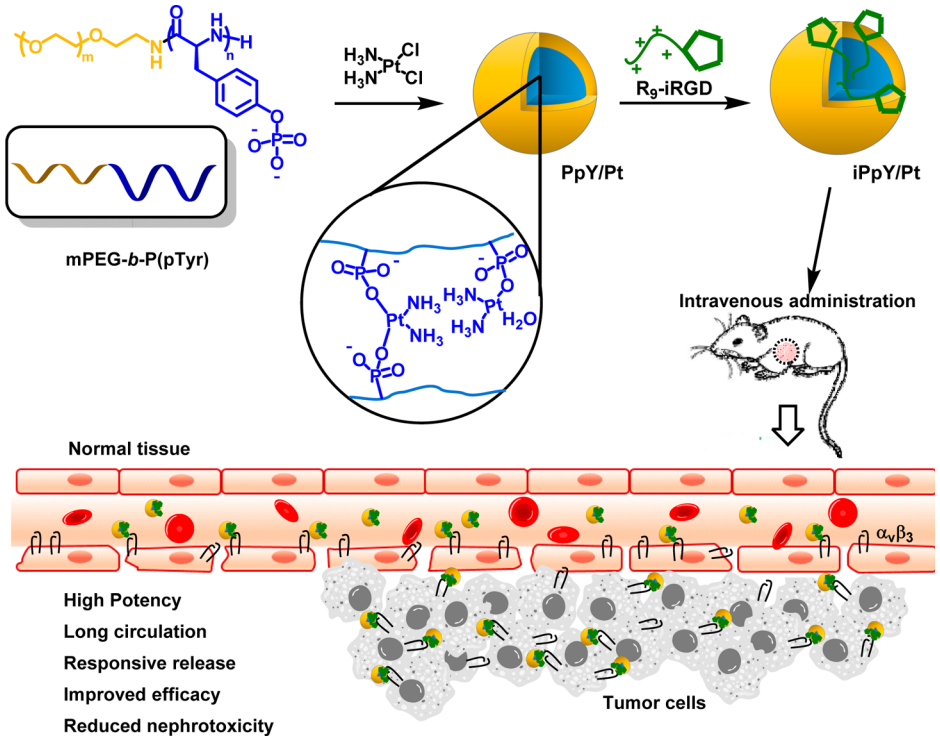

Figure 1. Synthesis of PpY/Pt and iPpY/Pt micelles.

Table 1. Characterization of PpY/Pt and iPpY/Pt Micelles

	size ± PDI (nm)				
nanoparticle	in PBS	in water	zeta-potential (mV)	drug loading (wt %)	loading efficiency (%)
PpY/Pt	43 ± 3	47 ± 2	−21.5	13	85
iPpY/Pt	35 ± 1	40 ± 1	−4.2	10	85

2.17. Blood Biochemical Analyses. At the end of therapy study, 200 μL of blood without anticoagulant was drawn from each mouse via enucleation method and centrifuged at 4000 *g* for 15 min. The serum was collected to detect the clinical biochemical parameters by corresponding kits (Cordor Medical).

3. RESULTS AND DISCUSSION

3.1. Synthesis and Characterization. To prepare the CDDP-loaded micelle (termed as PpY/Pt), mPEG-*b*-PpY (M_W of mPEG = 5000 Da, DP of PpY = 15; characterization results available in the Supporting Information, SI, Figure S1) was mixed with a freshly prepared *cis*-[Pt(II) $(NH_3)_2(H_2O)_2$]-$(NO_3)_2$ solution under rigorous stirring at room temperature (Figure 1). The PpY/Pt micelle, purified by ultracentrifugation, exhibited a −21.5 mV zeta-potential and a narrowly dispersed hydrodynamic sizes of ∼47 nm in water as determined by dynamic light scattering (DLS, Table 1 and Figure 2A). Transmission electron microscopy (TEM) study with uranyl acetate staining revealed that the average diameter of the micellar core was ∼20−25 nm (Figure 2A, inset). The ^{31}P NMR spectra of PEG-*b*-PpY and PpY/Pt implied the phosphato-platinum bonding as shown by a clear shift of the phosphate peak (Figure S2). Circular dichroism (CD) spectroscopy showed that the PpY domain underwent a disorder-to-order conformational transition upon phosphato-platinum complexation, suggesting the presence of peptidic hydrogen bonding during the micelle formation (Figure S3). To install a tumor targeting modality and engineer the surface to a near neutral state, we coated the highly negatively charged PpY/Pt micelle with a short peptide denoted as R_9-iRGD, which contains a cationic oligoarginine for electrostatic anchoring and an iRGD motif for tumor homing and penetration (Figure 1).[57−59] The resultant micelle, termed as iPpY/Pt, showed a substantially increased zeta potential from −21.5 to −4.2 mV. Interestingly, the hydrodynamic size of iPpY/Pt determined by DLS shrank slightly from 47 to 39 nm (Figure 2B). Thus, it seems the sizes of both micelles were in an optimal range for tumor accumulation and penetration.[34,60] ICP-MS determined the drug loading contents (DLC) of ∼10−13% and drug loading efficiencies (DLE) of ∼85% for both micelles (Table 1). Notably, mPEG-*b*-PpY bearing a longer PpY block (DP = 30) resulted in similar results (data not shown).

3.2. Stability. The two micelles were highly stable under physiological condition and could withstand various environmental stresses. For instance, both micelles remained almost unchanged in PBS, DMEM, and DMEM with 10% FBS for at least 1 week without aggregation or dissociation (Figures 2C and S4). In comparison, nanoparticles such as the FDA-approved PEG-*b*-poly(lactide-*co*-glycolide) usually cannot be stably stored under such conditions.[61,62] To examine whether the micelles can keep their integrities under highly diluted conditions (e.g., upon administration to the body), PpY/Pt at 200 μg/mL (Pt concentration) was diluted 10 and 100 times in PBS. Interestingly, the micelles displayed almost the same sizes and surface properties at all concentrations 3 days after dilution

DOI: 10.1021/acsami.7b03686
ACS Appl. Mater. Interfaces 2017, 9, 17757−17768

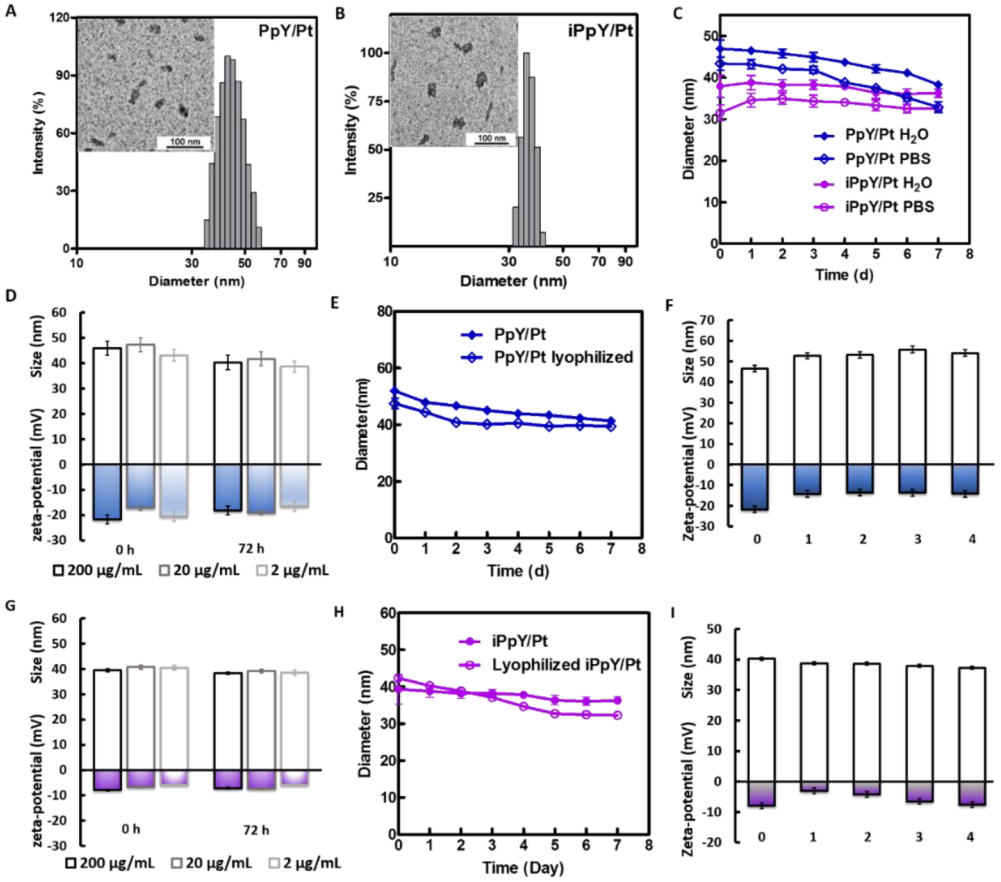

Figure 2. Stability of micelles. (A,B) Sizes of PpY/Pt (A) and iPpY/Pt (B) determined by DLS and TEM (inset). (C) Sizes of PpY/Pt and iPpY/Pt in water and PBS over time. (D and G) Sizes and zeta-potential of PpY/Pt (D) and iPpY/Pt (G) at different dilution factors over a period of 72 h. (E and H) Sizes of resuspended of PpY/Pt (E) and iPpY/Pt (H) after lyophilization over 1 week. (F and I) Sizes and zeta-potential of resuspended PpY/Pt (F) and iPpY/Pt (I) subjected to 4 cycles of lyophilization. Data were expressed as means ± SD from three independent experiments.

(Figure 2D). To assess their stability against lyophilization stress, PpY/Pt was freeze-dried and reconstituted in water. Again, DLS examination indicated that the size and zeta potential of the resuspended micelle kept unchanged for more than 1 week in PBS (Figure 2E). Moreover, no obvious change on the size and zeta potentials was observed for PpY/Pt undergoing repetitive cycles of lyophilization and resuspension (Figure 2F). It is worth noting that we obtained these results without special handling protocol and lyoprotectant, which are normally necessities for nanoparticle reconstiution.[61,63] Similar results were also observed for iPpY/Pt (Figure 2G–I). These remarakable characters were uncommon in conventional nanosystems and could largely facilitate the clinical translation of the micelles. The unusual high stability was provisionally attributed to a combinatory result of the $\pi-\pi$ stacking derived from phenyl segment and the ordered conformation of PpY after CDDP loading, which might stabilize the micellar core in a way similar to what the helical bundle does for CDDP-loaded PEG-*b*-PLG micelles.[48]

3.3. Release Kinetics and Trigger Responsiveness. Next, we studied the release kinetics of the micelles in DMEM cell culture medium with 10% FBS at 37 °C. As illustrated in Figures 3A and S5, PpY/Pt depicted a slow and sustained drug release profile with a plateau of total ~70% platinum released at ~72 h, and the addition of R_9-iRGD did not affect the release kinetics as evidenced by the almost identical release curves of iPpY/Pt and PpY/Pt (Figure 3A). Moreover, the drug release profile of PpY/Pt was not affected by the initial micellar concentrations (Figure 3B), implying an unlikelihood of burst release upon administration to the body. Acid promoted drug release, perhaps due to the protonation of phosphotyrosine ($pK_a \approx 5.8-6.0$), was validated using PpY/Pt in PBS buffers (Figure 3C). Most interestingly, we unexpectedly found that PpY/Pt displayed a substantially faster and more profound drug release upon incubation with high level of ATP, but not GTP, CTP, or UTP (Figure 3D). This result is intriguing because it implies the micelles could potentially illicit more potent killing to cancer cells that are known to have high intracellular ATP concentrations.[64,65] Although the exact mechanism of action for this responsiveness is still under investigation in our laboratory, one possible hypothesis is that both adenine and phosphate of ATP were involved in extracting platinum from PpY.[66] Together, the results advocated the notion that the micelles could release platinum in a slow and sustained manner under normal physiology conditions, and unload the cargo more rapidly in response to pathological or intracellular signals.

3.4. Cellular and Genomic DNA Platination. Next, we investigated the internalization of platinum in both cell lysates and genomic DNA by separately treating cells with CDDP or micelles at varied concentrations and incubation duration. HeLa and 4T1 were selected for their overexpressed RGD-receptor integrin $\alpha_v\beta_3$ and neuropilin-1.[67,68] ICP-MS measurement indicated time-dependent increases in platinum internalization from 4 to 36 h for all groups (Figure 4A,B).

DOI: 10.1021/acsami.7b03686
ACS Appl. Mater. Interfaces 2017, 9, 17757–17768

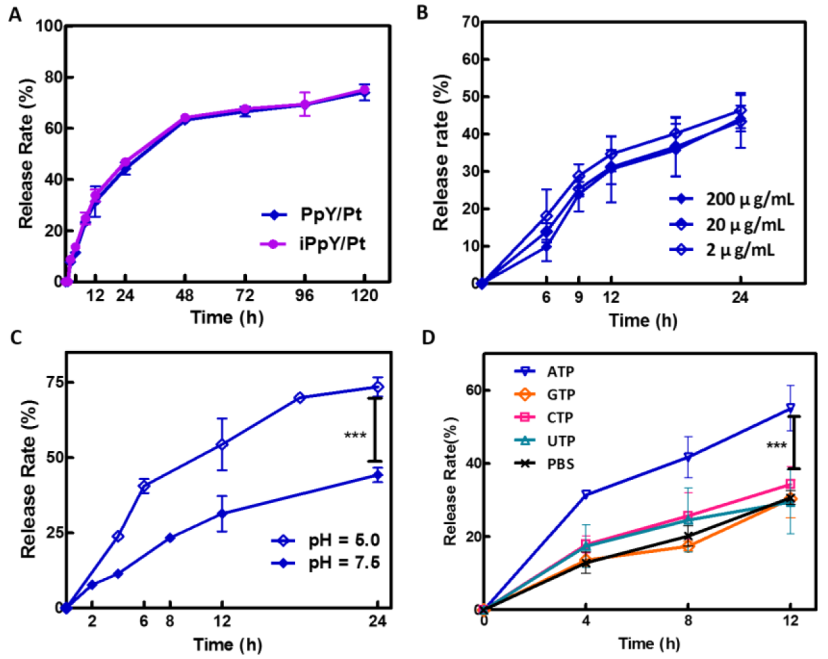

Figure 3. Release kinetics and stimuli-responsiveness. (A) Release kinetics of PpY/Pt and iPpY/Pt in DMEM supplemented with 10% FBS at 37 °C. (B) Release kinetics of PpY/Pt at varied initial concentrations. (C) Release kinetics of PpY/Pt at pH 5.0 and 7.5 in PBS. (D) Release kinetics of PpY/Pt in PBS, or in PBS containing 10 mM ATP, GTP, CTP, or UTP. Experiments were performed in dialysis bags against designated buffers (1.0 mL micelle against 99 mL buffer for A–C and 0.10 mL micelle against 9.9 mL buffer for (D) and the released platinum contents were measured by ICP-MS. Data were expressed as means ± SD from three independent experiments. *P* value was determined by two-way ANOVA analysis: * $p < 0.05$, ** $p < 0.001$, *** $p < 0.0001$.

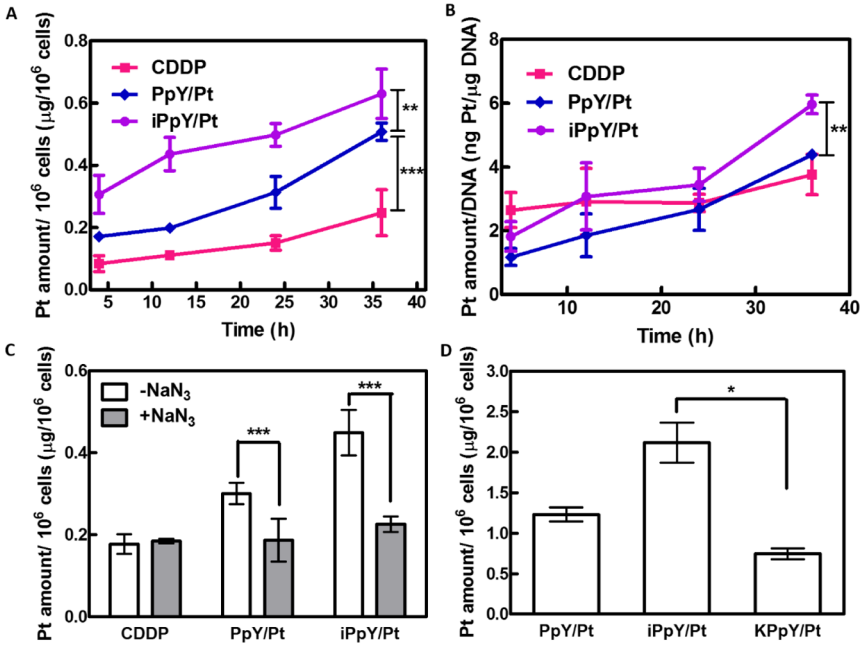

Figure 4. Cellular internalization of CDDP, PpY/Pt and iPpY/Pt measured by ICP-MS. (A,B) Time-dependent accumulation of Pt in whole-cell lysate (A) and genomic DNA (B) of HeLa cells; cells were treated with each group at10 μM platinum. (C) Pt accumulation in sodium azide pretreated cells; cells were treated with 10 mM NaN_3 before receiving each group at 10 μM platinum. (D) Cellular Pt accumulation in PpY/Pt, iPpY/Pt, or KPpY/Pt treated cells; cells were treated with each group at 30 μM for 4 h. Data were expressed as means ± SD from three independent experiments. The *p* value was determined by two-way ANOVA analysis: * $p < 0.05$, ** $p < 0.001$, *** $p < 0.0001$.

Surprisingly, both micelle-treated cells showed higher Pt concentrations in the lysate compared to those incubated with CDDP, and iPpY/Pt group exhibited the greatest level of cellular Pt (Figure 4A). In genomic DNA, however, the patterns of CDDP group and micellar groups were different. Specifically, the DNA platination level was almost constant over 36 h in CDDP-treated cells, whereas a time-dependent growth pattern in DNA platination was evident for both micellar treatments, with iPpY/Pt group again showed the highest Pt contents among the three at 36 h (Figure 4B). In contrast to

DOI: 10.1021/acsami.7b03686
ACS Appl. Mater. Interfaces 2017, 9, 17757–17768

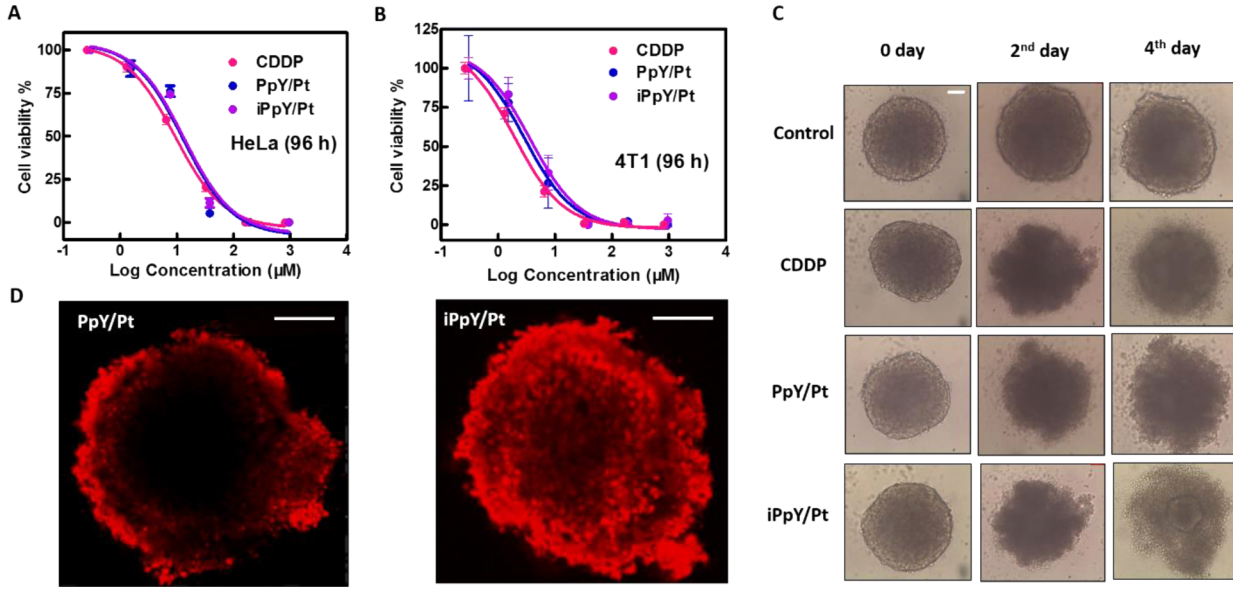

Figure 5. In vitro anticancer activity of CDDP, PpY/Pt and iPpY/Pt. (A,B) representative viability curves in 2D cell culture; Hela (A) and 4T1 (B) cells were treated with each therapy and incubated for 96 h; data were expressed as means ± SD from five independent experiments. (C) Microscopy photographs of CDDP, PpY/Pt, and iPpY/Pt treated 4T1 cells in a 3D multicellular tumor spheroids (MCTS) model. Scale bar: 100 μm. D) CLSM photographs of the 4T1 spheroidal cross sections treated by Cy5-labeled PpY/Pt and iPpY/Pt; scale bar: 200 μm.

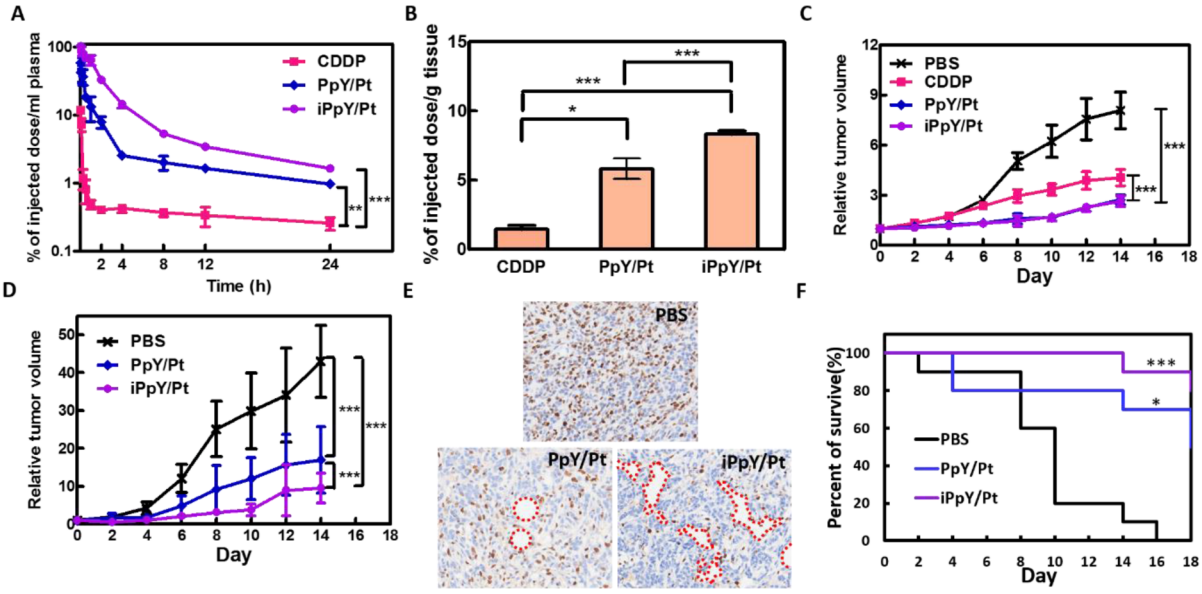

Figure 6. In vivo antitumor efficacy of PpY/Pt and iPpY/Pt. (A,B) pharmacokinetic (A) and tumor accumulation (B) of CDDP, PpY/Pt, and iPpY/Pt in 4T1 tumor-bearing BALB/C mice (n = 5); mice bearing orthotropic mammary 4T1tumors received each therapy at a single injection dose of 100 μg CDDP/mouse; the Pt concentration was measured by ICP-MS; % of injected dose/mL plasma = 100% × (the measured drug content in 1 mL of plasma/total content of injected drug); % of injected dose/g tissue = 100% × (the measured drug content in 1 g of tumor tissue/total content of injected drug). (C) Antitumor efficacy of CDDP, PpY/Pt, and iPpY/Pt in a xenograft mouse model bearing HeLa tumors (n = 5); mice received each therapy at a 1.5 mg/kg dose every other day via tail-vein route for a total of 5 injections. (D−F) Tumor size (D), histology (K_i-67 staining) of tumor (E), and survival rate (F) of PBS, PpY/Pt, or iPpY/Pt treated mice (n = 10); mice bearing orthotropic mammary 4T1 tumors received each therapy at a 3.0 mg/kg dose every other day via tail-vein route for a total of 7 injections. Red dotted lines circled representative damaged tumor tissues. Data were expressed as means ± SD; P value was determined by two-way ANOVA analysis: * $p < 0.05$, ** $p < 0.001$, *** $p < 0.0001$.

CDDP, whose nuclues transportation could be achieved by diffusion, the slow but steadily increased DNA platination pattern of the two micelles may be related to their particulate nature and sustained release kinetics. To interrogate the internalization mechanism of the micelles, cells were pretreated with 10 mM NaN_3. Unlike the CDDP group, both micellar groups showed dramatically decreased platinum uptake in the cell lysates after NaN_3 treatment (Figure 4C), suggesting energy-dependent pathways such as endocytosis. To validate the receptor-dependent internalization of iPpY/Pt, a control micelle termed as KPpY/Pt was prepared by coating PpY/Pt with a nontargeting peptide denoted as R_9-iKGD, which has an almost identical sequence to R_9-iRGD except that the targeting RGD motif was mutated to a nontargeting KGD. Incubation of

DOI: 10.1021/acsami.7b03686
ACS Appl. Mater. Interfaces 2017, 9, 17757−17768

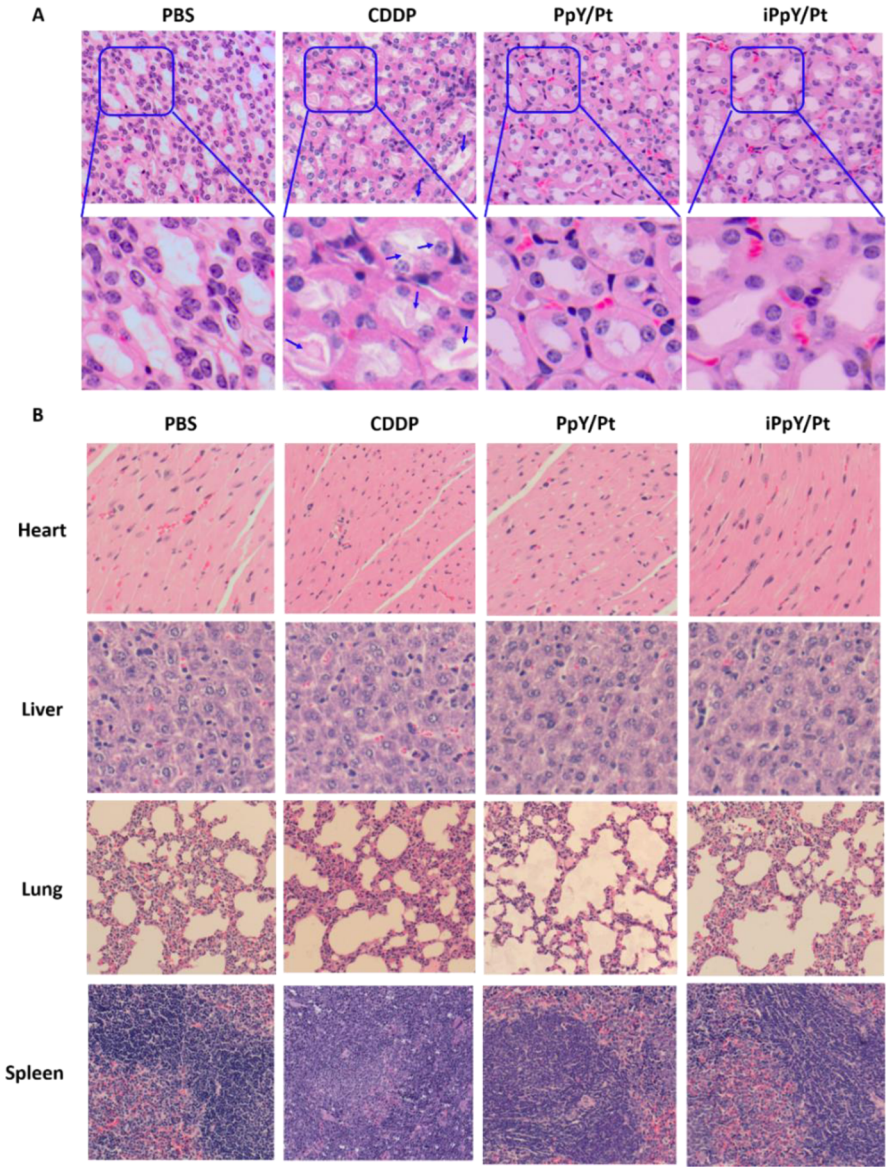

Figure 7. Histology of major organs such as kidney (A), heart, liver, lung, and spleen (B) dissected from mice receiving PBS, CDDP, PpY/Pt, or iPpY/Pt treatment. Arrows show representative damaged and exfoliated renal tubular epithelial cells.

this nontargeting KPpY/Pt micelle led to a much lower level of cellular Pt compared to the iPpY/Pt treatment (Figure 4D), confirming the importance of the RGD sequence. Dose-dependent internalization of the micelles was also observed as determined by both ICP-MS and FACS (Figures S6 and S7).

3.5. In Vitro Anticancer Activity in 2D Cell Culture and 3D MCTS. The in vitro anticancer toxicity of the micelles was evaluated in several human and mouse cancer cell lines including Hela (human cervical cancer), HepG2 (human liver cancer), SaoS-2 (human osteosarcoma), U2-OS (human osteosarcoma), 4T1 (mouse breast cancer), A549 (human lung cancer), and SKOV-3 (human ovarian cancer). PpY/Pt and iPpY/Pt were almost equally potent compared to CDDP in both Hela and 4T1 when incubated for 72 (Figure S8 and Table S1) or 96 h (Figure 5A,B and Table S1). With less incubation time (e.g., 48 h), however, both micelles were 2−3 fold less potent than CDDP in most cells tested (Figure S9 and Table S2). This time-dependent toxicity pattern of the micelles agreed well with their gradually increased DNA platination level shown in Figure 4B. The reason for the comparable cytotoxicity of the two micelles in all cell lines tested, however, is currently unclear (Tables S1 and S2).[59] Notably, PpY/Pt resuspended from lyophilized powders displayed almost identical toxicity curves with the freshly prepared micelle, which reconfirmed the lyopreservation ability (Figure S10). Overall, the micelles were considerably more potent than most carboxylato-platinum based delivery systems.[35]

To overcome the limitation of 2D cell culture, we further assessed the micellar anticancer activity by employing an in vitro 3D model mimicking solid tumors, namely multicellular tumor spheroids (MCTS). Specifically, the spheroids of 4T1 cells, with an average diameter of ∼600 μm, were incubated with CDDP or micelles at 50 μM for up to 4 days. The antiproliferative efficacies of the drugs were evaluated by microscopy observation. Different from the 2D cell culture results, the iPpY/Pt treatment led to the highest toxicity in 3D MCTS, as evidenced by both the morphological change and loss of integrity of the spheroid (Figure 5C). The superior

DOI: 10.1021/acsami.7b03686
ACS Appl. Mater. Interfaces 2017, 9, 17757−17768

antiproliferative activity of iPpY/Pt prompt us to test the iRGD promoted tumor penetration hypothesis by using confocal laser scanning microscopy (CLSM). Indeed, high intensity fluorescence lit up in both the periphery and core of the spheroidal cross section for cells treated with Cy5-labeled iPpY/Pt; in sharp contrast, fluorescence could only be observed in the outer layer for PpY/Pt-treated spheroids (Figure 5D).

3.6. In Vivo Pharmacokinetics and Tumor Accumulation. A few major advantages of nanomedicines over small molecular drugs were their prolonged circulation half-lives, enhanced permeation and retention (EPR) effect at tumor site, and tailored active targeting. To this end, we intravenously injected CDDP or micelles at ~3.0 mg/kg (Pt concentration) to Balb/c mice bearing orthotropic mammary 4T1 tumors and then measured the platinum contents in both plasma and tumors at various time intervals by using ICP-MS. As shown in Figure 6A, the Pt content in plasma plunged down to only 0.5% of the injected dose per milliliter (ID/mL) within 1.0 h for the CDDP group, as compared to 13.2 and 64.6% ID/mL for PpY/Pt and iPpY/Pt at the same time point, respectively. At 24 h, the plasma platinum contents of CDDP, PpY/Pt, and iPpY/Pt groups were determined as 0.26, 0.97, and 1.26% ID/mL. The half-lives of them were 0.4, 4.0, and 4.2 h, respectively. In tumors, PpY/Pt and iPpY/Pt treatments showed 5.8 and 8.3% of the injected dose per gram of tissue (ID/g) 24 h post injection, which was approximately ~4.1 ($*P < 0.05$) and 5.9 fold ($***P < 0.001$) higher than the CDDP group, respectively (Figure 6B). Together, the results indicated that micellerization prolonged the half-lives and increased tumor accumulation of CDDP, and R_9-iRGD coating further improved such effects for iPpY/Pt.

3.7. In Vivo Efficacy. Next, we examined the in vivo efficacy of the micelles by using a xenograft HeLa tumor model. BALB/c nude mice bearing ~50 mm^3 s.c. implanted HeLa tumors ($n = 5$) received PBS, CDDP or micelles (1.5 mg Pt/kg) every other day via tail vein injection. Whereas the HeLa tumor in the PBS group gradually progressed, both micelles outpermed CDDP in tumor growth inhibition at the same platinum dosage (Figure 6C,$*P < 0.001$). No significant body-weight loss was observed (Figure S11).

With this success, we continued to evaluate the in vivo efficacy by using a more aggressive orthotropic mammary 4T1 tumors model in BALB/c mice. When the tumors reached an average size of 50 mm^3, mice ($n = 10$) separately received PBS, PpY/Pt or iPpY/Pt therapy at a 3.0 mg/kg dose every other day via tail-vein administration. As expected, the average tumor size of the PBS group rapidly exceeded 1000 mm^3 on day 8, which necessitates mandatory euthanasia; in contrast, mice treated with PpY/Pt or iPpY/Pt on the same day showed an average tumor size of only 342 and 129 mm^3, respectively (Figure 6D). Furthermore, histology analysis of the extracted tumors showed that iPpY/Pt treatment gave more observed empty holes and less K_i-67 staining compared to the other two groups, which indicated higher degree of tumor tissue damage and more effective inhibition of cancer cell proliferation, respectively (Figure 6E). In consistent with the tumor inhibition, the survival rate of the mice on day 16 after treatment were extended from 0% for the PBS group to 70 and 90% for PpY/Pt and iPpY/Pt group, respectively (Figure 6F). Notably, and in good agreement with previously reported results,[51] mice received CDDP therapy at 3.0 mg/kg suffered severe side effects and significant body-weight loss (data not shown), underscoring the improved therapeutic index of our micelles.

3.8. In Vivo Safety. To evaluate the in vivo safety profile of our delivery system, we performed histology studies and blood biochemical analysis. Importantly, CDDP treatment led to devastating kidney damage for its well-known nephrotoxicity as evidenced by the damaged and exfoliated renal tubular epithelial cells; in contrast, both micellar treatments at the same platinum dosage did not show significant tissue damage (Figure 7A), which was further confirmed by the blood urea nitrogen (BUN) parameter analysis (Figure S12). Moreover, we observed no major damage in organs such as heart, liver, spleen, and lung for both micellar groups (Figure 7B).

4. CONCLUSIONS

In summary, we conceived and prepared two CDDP-loaded PpY/Pt and iPpY/Pt micelles based on a bioinspired and biodegradable polymer mPEG-*b*-PpY. The micelles, which relied on the phosphato-platinum bonding, showed good drug loading, optimal sizes for nanomedicine, and unusual high stability under physiological conditions and against environmental stresses. Moreover, the micelles displayed faster drug release in responding to pathological and intracellular signals, which could be leveraged for on-demand intracellular delivery. In vitro, the micelles exhibited higher anticancer activity than conventional carboxylato-platinum based nanocarriers; the iRGD functionalized iPpY/Pt demonstrated deeper tumor penetration and higher potency compared to PpY/Pt in a 3D MCTS model. In vivo, both micelles showed prolonged circulation half-lives, enhanced tumor accumulation, improved antitumor efficacy and better tolerance than CDDP. Furthermore, iPpY/Pt was significantly more potent in inhibiting tumor growth than PpY/Pt in the orthotropic 4T1 model. Taken together, the present work demonstrated for the first time that phosphato-platinum complexation can be harnessed for effective delivery of Pt(II)-based drugs. Given the versatility and strong metal binding ability of phosphate, PpY could be a promising vehicle for a vast number of anticancer metallodrugs.[69,70]

■ ASSOCIATED CONTENT

Supporting Information

The Supporting Information is available free of charge on the ACS Publications website at DOI: 10.1021/acsami.7b03686.

^{1}H NMR and GPC curve of mPEG-*b*-P(pOEtTyr)$_{15}$, ^{1}H NMR of mPEG-*b*-PpY, ^{31}P NMR and CD sepctra of mPEG-*b*-PpY and PpY/Pt, dose-dependent cellular internalization of CDDP, PpY/Pt, and iPpY/Pt, relative cell viability curves and IC50s of CDDP, PpY/Pt, and iPpY/Pt for 48, 72, 96 h, relative cell viability curves of PpY/Pt before and after lyophilization, relative body weight of mice bearing different tumor models, blood biochemical analysis (PDF)

■ AUTHOR INFORMATION

Corresponding Authors

*E-mail: weiwei@ipe.ac.cn (W.W.).
*E-mail: chemhualu@pku.edu.cn (H.L.).

ORCID

Shengtao Yang: 0000-0001-6795-8879
Hua Lu: 0000-0003-2180-3091

Author Contributions

‖Y.Q.H. and Y.Y.W. contributed equally to this work.

DOI: 10.1021/acsami.7b03686
ACS Appl. Mater. Interfaces 2017, 9, 17757−17768

Funding

This work was financially supported by National Key Research and Development Program of China (2016YFA0201400). We thank the grants from National Natural Science Foundation of China (21434008 for H.L. and 21622608 for W.W.), the Open Funding Project of the State Key Laboratory of Biochemical Engineering (2015KF-01) and Beijing Talents Fund (2015000021223ZK20 for W.W.).

Notes

The authors declare no competing financial interest.

■ ACKNOWLEDGMENTS

We gratefully thank the helpful suggestions from Prof. Kazunori Kataoka and Prof. Peng Mi.

■ REFERENCES

(1) Kelland, L. The Resurgence of Platinum-Based Cancer Chemotherapy. *Nat. Rev. Cancer* **2007**, *7* (8), 573−584.

(2) Johnstone, T. C.; Suntharalingam, K.; Lippard, S. J. The Next Generation of Platinum Drugs: Targeted Pt(II) Agents, Nanoparticle Delivery, and Pt(IV) Prodrugs. *Chem. Rev.* **2016**, *116* (5), 3436−3486.

(3) Zheng, Y. R.; Suntharalingam, K.; Johnstone, T. C.; Yoo, H.; Lin, W.; Brooks, J. G.; Lippard, S. J. Pt(IV) Prodrugs Designed to Bind Non-Covalently to Human Serum Albumin for Drug Delivery. *J. Am. Chem. Soc.* **2014**, *136* (24), 8790−8798.

(4) Liu, Z. B.; Chen, X. Y. Simple Bioconjugate Chemistry Serves Great Clinical Advances: Albumin as a Versatile Platform for Diagnosis and Precision Therapy. *Chem. Soc. Rev.* **2016**, *45* (5), 1432−1456.

(5) Patra, M.; Johnstone, T. C.; Suntharalingam, K.; Lippard, S. J. A Potent Glucose-Platinum Conjugate Exploits Glucose Transporters and Preferentially Accumulates in Cancer Cells. *Angew. Chem., Int. Ed.* **2016**, *55* (7), 2550−2554.

(6) Pathak, R. K.; Marrache, S.; Choi, J. H.; Berding, T. B.; Dhar, S. The Prodrug Platin-A: Simultaneous Release of Cisplatin and Aspirin. *Angew. Chem., Int. Ed.* **2014**, *53* (7), 1963−1967.

(7) Awuah, S. G.; Zheng, Y. R.; Bruno, P. M.; Hemann, M. T.; Lippard, S. J. A Pt(IV) Pro-Drug Preferentially Targets Indoleamine-2,3-dioxygenase, Providing Enhanced Ovarian Cancer Immuno-Chemotherapy. *J. Am. Chem. Soc.* **2015**, *137* (47), 14854−14857.

(8) Wang, X.; Guo, Z. Targeting and Delivery of Platinum-Based Anticancer Drugs. *Chem. Soc. Rev.* **2013**, *42* (1), 202−224.

(9) Butler, J. S.; Sadler, P. J. Targeted Delivery of Platinum-Based Anticancer Complexes. *Curr. Opin. Chem. Biol.* **2013**, *17* (2), 175−188.

(10) Li, S. D.; Chen, Y. C.; Hackett, M. J.; Huang, L. Tumor-Targeted Delivery of siRNA by Self-Assembled Nanoparticles. *Mol. Ther.* **2008**, *16* (1), 163−169.

(11) He, C. B.; Poon, C.; Chan, C.; Yamada, S. D.; Lin, W. B. Nanoscale Coordination Polymers Codeliver Chemotherapeutics and siRNAs to Eradicate Tumors of Cisplatin-Resistant Ovarian Cancer. *J. Am. Chem. Soc.* **2016**, *138* (18), 6010−6019.

(12) Xu, X.; Xie, K.; Zhang, X. Q.; Pridgen, E. M.; Park, G. Y.; Cui, D. S.; Shi, J.; Wu, J.; Kantoff, P. W.; Lippard, S. J.; Langer, R.; Walker, G. C.; Farokhzad, O. C. Enhancing Tumor Cell Response to Chemotherapy Through Nanoparticle-Mediated Codelivery of siRNA and Cisplatin Prodrug. *Proc. Natl. Acad. Sci. U. S. A.* **2013**, *110* (46), 18638−18643.

(13) Shen, S.; Sun, C. Y.; Du, X. J.; Li, H. J.; Liu, Y.; Xia, J. X.; Zhu, Y. H.; Wang, J. Co-Delivery of Platinum Drug and siNotch1 with Micelleplex for Enhanced Hepatocellular Carcinoma Therapy. *Biomaterials* **2015**, *70*, 71−83.

(14) Xiao, H.; Qi, R.; Li, T.; Awuah, S. G.; Zheng, Y.; Wei, W.; Kang, X.; Song, H.; Wang, Y.; Yu, Y.; Bird, M. A.; Jing, X.; Yaffe, M. B.; Birrer, M. J.; Ghoroghchian, P. P. Maximizing Synergistic Activity When Combining RNAi and Platinum-Based Anticancer Agents. *J. Am. Chem. Soc.* **2017**, *139* (8), 3033−3044.

(15) Miao, L.; Guo, S.; Zhang, J.; Kim, W. Y.; Huang, L. Nanoparticles with Precise Ratiometric Co-Loading and Co-Delivery of Gemcitabine Monophosphate and Cisplatin for Treatment of Bladder Cancer. *Adv. Funct. Mater.* **2014**, *24* (42), 6601−6611.

(16) Hu, Q.; Sun, W.; Wang, C.; Gu, Z. Recent Advances of Cocktail Chemotherapy by Combination Drug Delivery Systems. *Adv. Drug Delivery Rev.* **2016**, *98*, 19−34.

(17) Ashley, C. E.; Carnes, E. C.; Phillips, G. K.; Padilla, D.; Durfee, P. N.; Brown, P. A.; Hanna, T. N.; Liu, J. W.; Phillips, B.; Carter, M. B.; Carroll, N. J.; Jiang, X. M.; Dunphy, D. R.; Willman, C. L.; Petsev, D. N.; Evans, D. G.; Parikh, A. N.; Chackerian, B.; Wharton, W.; Peabody, D. S.; Brinker, C. J. The Targeted Delivery of Multicomponent Cargos to Cancer Cells by Nanoporous Particle-Supported Lipid Bilayers. *Nat. Mater.* **2011**, *10* (5), 389−397.

(18) Lee, S. M.; O'Halloran, T. V.; Nguyen, S. T. Polymer-Caged Nanobins for Synergistic Cisplatin-Doxorubicin Combination Chemotherapy. *J. Am. Chem. Soc.* **2010**, *132* (48), 17130−17138.

(19) Li, M. Q.; Tang, Z. H.; Lv, S. X.; Song, W. T.; Hong, H.; Jing, X. B.; Zhang, Y. Y.; Chen, X. S. Cisplatin Crosslinked pH-Sensitive Nanoparticles for Efficient Delivery of Doxorubicin. *Biomaterials* **2014**, *35* (12), 3851−3864.

(20) Xiao, H. H.; Song, H. Q.; Yang, Q.; Cai, H. D.; Qi, R. G.; Yan, L. S.; Liu, S.; Zheng, Y. H.; Huang, Y. B.; Liu, T. J.; Jing, X. B. A Prodrug Strategy to Deliver Cisplatin(IV) and Paclitaxel in Nanomicelles to Improve Efficacy and Tolerance. *Biomaterials* **2012**, *33* (27), 6507−6519.

(21) Dhar, S.; Daniel, W. L.; Giljohann, D. A.; Mirkin, C. A.; Lippard, S. J. Polyvalent Oligonucleotide Gold Nanoparticle Conjugates as Delivery Vehicles for Platinum(IV) Warheads. *J. Am. Chem. Soc.* **2009**, *131* (41), 14652−14653.

(22) Wan, X. J.; Zhang, G. Y.; Liu, S. Y. pH-Disintegrable Polyelectrolyte Multilayer-Coated Mesoporous Silica Nanoparticles Exhibiting Triggered Co-Release of Cisplatin and Model Drug Molecules. *Macromol. Rapid Commun.* **2011**, *32* (14), 1082−1089.

(23) Zhou, F. Y.; Feng, B.; Yu, H. J.; Wang, D. G.; Wang, T. T.; Liu, J. P.; Meng, Q. S.; Wang, S. L.; Zhang, P. C.; Zhang, Z. W.; Li, Y. P. Cisplatin Prodrug-Conjugated Gold Nanocluster for Fluorescence Imaging and Targeted Therapy of the Breast Cancer. *Theranostics* **2016**, *6* (5), 679−687.

(24) Ma, P.; Xiao, H.; Yu, C.; Liu, J.; Cheng, Z.; Song, H.; Zhang, X.; Li, C.; Wang, J.; Gu, Z.; Lin, J. Enhanced Cisplatin Chemotherapy by Iron Oxide Nanocarrier-Mediated Generation of Highly Toxic Reactive Oxygen Species. *Nano Lett.* **2017**, *17* (2), 928−937.

(25) Kumar, A.; Huo, S. D.; Zhang, X.; Liu, J.; Tan, A.; Li, S. L.; Jin, S. B.; Xue, X. D.; Zhao, Y. Y.; Ji, T. J.; Han, L.; Liu, H.; Zhang, X. N.; Zhang, J. C.; Zou, G. Z.; Wang, T. Y.; Tang, S. Q.; Liang, X. J. Neuropilin-1-Targeted Gold Nanoparticles Enhance Therapeutic Efficacy of Platinum(IV) Drug for Prostate Cancer Treatment. *ACS Nano* **2014**, *8* (5), 4205−4220.

(26) Huang, C.; Neoh, K. G.; Xu, L. Q.; Kang, E. T.; Chiong, E. Polymeric Nanoparticles with Encapsulated Superparamagnetic Iron Oxide and Conjugated Cisplatin for Potential Bladder Cancer Therapy. *Biomacromolecules* **2012**, *13* (8), 2513−2520.

(27) He, C. B.; Lu, K. D.; Liu, D. M.; Lin, W. B. Nanoscale Metal-Organic Frameworks for the Co-Delivery of Cisplatin and Pooled siRNAs to Enhance Therapeutic Efficacy in Drug-Resistant Ovarian Cancer Cells. *J. Am. Chem. Soc.* **2014**, *136* (14), 5181−5184.

(28) Rieter, W. J.; Pott, K. M.; Taylor, K. M. L.; Lin, W. B. Nanoscale Coordination Polymers for Platinum-Based Anticancer Drug Delivery. *J. Am. Chem. Soc.* **2008**, *130* (35), 11584−11585.

(29) Guo, S.; Wang, Y.; Miao, L.; Xu, Z.; Lin, C. M.; Zhang, Y.; Huang, L. Lipid-Coated Cisplatin Nanoparticles Induce Neighboring Effect and Exhibit Enhanced Anticancer Efficacy. *ACS Nano* **2013**, *7* (11), 9896−9904.

(30) Cao, Z. H.; Tong, R.; Mishra, A.; Xu, W. C.; Wong, G. C. L.; Cheng, J. J.; Lu, Y. Reversible Cell-Specific Drug Delivery with Aptamer-Functionalized Liposomes. *Angew. Chem., Int. Ed.* **2009**, *48* (35), 6494−6498.

(31) Li, Q.; Tian, Y. T.; Li, D. D.; Sun, J. F.; Shi, D. L.; Fang, L.; Gao, Y.; Liu, H. Y. The Effect of Lipocisplatin on Cisplatin Efficacy and

DOI: 10.1021/acsami.7b03686
ACS Appl. Mater. Interfaces 2017, 9, 17757−17768

Nephrotoxicity in Malignant Breast Cancer Treatment. *Biomaterials* **2014**, *35* (24), 6462−6472.
(32) Dhar, S.; Kolishetti, N.; Lippard, S. J.; Farokhzad, O. C. Targeted Delivery of a Cisplatin Prodrug for Safer and More Effective Prostate Cancer Therapy *in vivo*. *Proc. Natl. Acad. Sci. U. S. A.* **2011**, *108* (5), 1850−1855.
(33) Callari, M.; Aldrich-Wright, J. R.; de Souza, P. L.; Stenzel, M. H. Polymers with Platinum Drugs and Other Macromolecular Metal Complexes for Cancer Treatment. *Prog. Polym. Sci.* **2014**, *39* (9), 1614−1643.
(34) Cabral, H.; Matsumoto, Y.; Mizuno, K.; Chen, Q.; Murakami, M.; Kimura, M.; Terada, Y.; Kano, M. R.; Miyazono, K.; Uesaka, M.; Nishiyama, N.; Kataoka, K. Accumulation of Sub-100 nm Polymeric Micelles in Poorly Permeable Tumours Depends on Size. *Nat. Nanotechnol.* **2011**, *6* (12), 815−823.
(35) Nishiyama, N.; Okazaki, S.; Cabral, H.; Miyamoto, M.; Kato, Y.; Sugiyama, Y.; Nishio, K.; Matsumura, Y.; Kataoka, K. Novel Cisplatin-Incorporated Polymeric Micelles Can Eradicate Solid Tumors in Mice. *Cancer Res.* **2003**, *63* (24), 8977−8983.
(36) Song, H. Q.; Xiao, H. H.; Zhang, Y.; Cai, H. D.; Wang, R.; Zheng, Y. H.; Huang, Y. B.; Li, Y. X.; Xie, Z. G.; Liu, T. J.; Jing, X. B. Multifunctional Pt(IV) Pro-Drug and Its Micellar Platform: To Kill Two Birds with One Stone. *J. Mater. Chem. B* **2013**, *1* (6), 762−772.
(37) Yang, X. Z.; Du, X. J.; Liu, Y.; Zhu, Y. H.; Liu, Y. Z.; Li, Y. P.; Wang, J. Rational Design of Polyion Complex Nanoparticles to Overcome Cisplatin Resistance in Cancer Therapy. *Adv. Mater.* **2014**, *26* (6), 931−936.
(38) Li, H. J.; Du, J. Z.; Du, X. J.; Xu, C. F.; Sun, C. Y.; Wang, H. X.; Cao, Z. T.; Yang, X. Z.; Zhu, Y. H.; Nie, S. M.; Wang, J. Stimuli-Responsive Clustered Nanoparticles for Improved Tumor Penetration and Therapeutic Efficacy. *Proc. Natl. Acad. Sci. U. S. A.* **2016**, *113* (15), 4164−4169.
(39) Yao, X. K.; Xie, C.; Chen, W. Z.; Yang, C. C.; Wu, W.; Jiang, X. Q. Platinum-Incorporating Poly(N-vinylpyrrolidone)-poly(aspartic acid) Pseudoblock Copolymer Nanoparticles for Drug Delivery. *Biomacromolecules* **2015**, *16* (7), 2059−2071.
(40) Shirbin, S. J.; Ladewig, K.; Fu, Q.; Klimak, M.; Zhang, X. Q.; Duan, W.; Qiao, G. G. Cisplatin-Induced Formation of Biocompatible and Biodegradable Polypeptide-Based Vesicles for Targeted Anticancer Drug Delivery. *Biomacromolecules* **2015**, *16* (8), 2463−2474.
(41) Song, W. T.; Li, M. Q.; Tang, Z. H.; Li, Q. S.; Yang, Y.; Liu, H. Y.; Duan, T. C.; Hong, H.; Chen, X. S. Methoxypoly(ethylene glycol)-block-Poly(L-glutamic acid)-Loaded Cisplatin and a Combination With iRGD for the Treatment of Non-Small-Cell Lung Cancers. *Macromol. Biosci.* **2012**, *12* (11), 1514−1523.
(42) Aryal, S.; Hu, C. M. J.; Zhang, L. F. Polymer-Cisplatin Conjugate Nanoparticles for Acid-Responsive Drug Delivery. *ACS Nano* **2010**, *4* (1), 251−258.
(43) Shen, W. J.; Luan, J. B.; Cao, L. P.; Sun, J.; Yu, L.; Ding, J. D. Thermogelling Polymer-Platinum(IV) Conjugates for Long-Term Delivery of Cisplatin. *Biomacromolecules* **2015**, *16* (1), 105−115.
(44) Song, W. T.; Tang, Z. H.; Zhang, D. W.; Zhang, Y.; Yu, H. Y.; Li, M. Q.; Lv, S. X.; Sun, H.; Deng, M. X.; Chen, X. S. Anti-Tumor Efficacy of c(RGDfK)-Decorated Polypeptide-Based Micelles Co-Loaded with Docetaxel and Cisplatin. *Biomaterials* **2014**, *35* (9), 3005−3014.
(45) Cabral, H.; Makino, J.; Matsumoto, Y.; Mi, P.; Wu, H. L.; Nomoto, T.; Toh, K.; Yamada, N.; Higuchi, Y.; Konishi, S.; Kano, M. R.; Nishihara, H.; Miura, Y.; Nishiyama, N.; Kataoka, K. Systemic Targeting of Lymph Node Metastasis Through the Blood Vascular System by Using Size-Controlled Nano carriers. *ACS Nano* **2015**, *9* (5), 4957−4967.
(46) Cai, L.; Xu, G.; Shi, C.; Guo, D.; Wang, X.; Luo, J. Telodendrimer Nanocarrier for Co-Delivery of Paclitaxel and Cisplatin: A Synergistic Combination Nanotherapy for Ovarian Cancer Treatment. *Biomaterials* **2015**, *37*, 456−468.
(47) Cabral, H.; Kataoka, K. Progress of Drug-Loaded Polymeric Micelles into Clinical Studies. *J. Controlled Release* **2014**, *190*, 465−476.
(48) Mochida, Y.; Cabral, H.; Miura, Y.; Albertini, F.; Fukushima, S.; Osada, K.; Nishiyama, N.; Kataoka, K. Bundled Assembly of Helical Nanostructures in Polymeric Micelles Loaded with Platinum Drugs Enhancing Therapeutic Efficiency Against Pancreatic Tumor. *ACS Nano* **2014**, *8* (7), 6724−6738.
(49) Murakami, M.; Cabral, H.; Matsumoto, Y.; Wu, S.; Kano, M. R.; Yamori, T.; Nishiyama, N.; Kataoka, K. Improving Drug Potency and Efficacy by Nanocarrier-Mediated Subcellular Targeting. *Sci. Transl. Med.* **2011**, *3* (64), 64ra2.
(50) Li, T. Y.; Smet, M.; Dehaen, W.; Xu, H. P. Selenium-Platinum Coordination Dendrimers with Controlled Anti-Cancer Activity. *ACS Appl. Mater. Interfaces* **2016**, *8* (6), 3609−3614.
(51) Paraskar, A. S.; Soni, S.; Chin, K. T.; Chaudhuri, P.; Muto, K. W.; Berkowitz, J.; Handlogten, M. W.; Alves, N. J.; Bilgicer, B.; Dinulescu, D. M.; Mashelkar, R. A.; Sengupta, S. Harnessing Structure-Activity Relationship to Engineer a Cisplatin Nanoparticle for Enhanced Antitumor Efficacy. *Proc. Natl. Acad. Sci. U. S. A.* **2010**, *107* (28), 12435−12440.
(52) Luan, J. B.; Shen, W. J.; Chen, C.; Lei, K. W.; Yu, L.; Ding, J. D. Selenium-Containing Thermogel for Controlled Drug Delivery by Coordination Competition. *RSC Adv.* **2015**, *5* (119), 97975−97981.
(53) Bose, R. N.; Maurmann, L.; Mishur, R. J.; Yasui, L.; Gupta, S.; Grayburn, W. S.; Hofstetter, H.; Salley, T. Non-DNA-Binding Platinum Anticancer Agents: Cytotoxic Activities of Platinum-Phosphato Complexes Towards Human Ovarian Cancer Cells. *Proc. Natl. Acad. Sci. U. S. A.* **2008**, *105* (47), 18314−18319.
(54) Li, S.-L.; Hou, Y.; Hu, Y.; Yu, J.; Wei, W.; Lu, H. Phosphatase-Triggered Cell-Selective Release of a Pt(IV)-Backboned Prodrug-Like Polymer for an Improved Therapeutic Index. *Biomater. Sci.* **2017**, DOI: 10.1039/C6BM00935B.
(55) Sun, Y.; Hou, Y.; Zhou, X.; Yuan, J.; Wang, J.; Lu, H. Controlled Synthesis and Enzyme-Induced Hydrogelation of Poly(L-phosphotyrosine)s via Ring-Opening Polymerization of alpha-Amino Acid N-Carboxyanhydride. *ACS Macro Lett.* **2015**, *4* (9), 1000−1003.
(56) Friedrich, J.; Seidel, C.; Ebner, R.; Kunz-Schughart, L. A. Spheroid-Based Drug Screen: Considerations and Practical Approach. *Nat. Protoc.* **2009**, *4* (3), 309−324.
(57) Sugahara, K. N.; Teesalu, T.; Karmali, P. P.; Kotamraju, V. R.; Agemy, L.; Girard, O. M.; Hanahan, D.; Mattrey, R. F.; Ruoslahti, E. Tissue-Penetrating Delivery of Compounds and Nanoparticles into Tumors. *Cancer Cell* **2009**, *16* (6), 510−520.
(58) Liu, Y.; Zhang, D.; Qiao, Z. Y.; Qi, G. B.; Liang, X. J.; Chen, X. G.; Wang, H. A Peptide-Network Weaved Nanoplatform with Tumor Microenvironment Responsiveness and Deep Tissue Penetration Capability for Cancer Therapy. *Adv. Mater.* **2015**, *27* (34), 5034−5042.
(59) Wang, X.; Zhen, X.; Wang, J.; Zhang, J. L.; Wu, W.; Jiang, X. Q. Doxorubicin Delivery to 3D Multicellular Spheroids and Tumors Based on Boronic Acid-Rich Chitosan Nanoparticles. *Biomaterials* **2013**, *34* (19), 4667−4679.
(60) Tang, L.; Yang, X.; Yin, Q.; Cai, K.; Wang, H.; Chaudhury, I.; Yao, C.; Zhou, Q.; Kwon, M.; Hartman, J. A.; Dobrucki, I. T.; Dobrucki, L. W.; Borst, L. B.; Lezmi, S.; Helferich, W. G.; Ferguson, A. L.; Fan, T. M.; Cheng, J. Investigating the Optimal Size of Anticancer Nanomedicine. *Proc. Natl. Acad. Sci. U. S. A.* **2014**, *111* (43), 15344−15349.
(61) Yin, Q.; Tong, R.; Xu, Y. X.; Baek, K.; Dobrucki, L. W.; Fan, T. M.; Cheng, J. J. Drug-Initiated Ring-Opening Polymerization of O-Carboxyanhydrides for the Preparation of Anticancer Drug-Poly(O-carboxyanhydride) Nanoconjugates. *Biomacromolecules* **2013**, *14* (3), 920−929.
(62) Cheng, J.; Teply, B. A.; Sherifi, I.; Sung, J.; Luther, G.; Gu, F. X.; Levy-Nissenbaum, E.; Radovic-Moreno, A. F.; Langer, R.; Farokhzad, O. C. Formulation of Functionalized PLGA-PEG Nanoparticles for *in vivo* Targeted Drug Delivery. *Biomaterials* **2007**, *28* (5), 869−876.
(63) Tong, R.; Yala, L. D.; Fan, T. M.; Cheng, J. J. The Formulation of Aptamer-Coated Paclitaxel-Polylactide Nanoconjugates and Their Targeting to Cancer Cells. *Biomaterials* **2010**, *31* (11), 3043−3053.

DOI: 10.1021/acsami.7b03686
ACS Appl. Mater. Interfaces 2017, 9, 17757−17768

(64) Zhou, Y.; Tozzi, F.; Chen, J.; Fan, F.; Xia, L.; Wang, J.; Gao, G.; Zhang, A.; Xia, X.; Brasher, H.; Widger, W.; Ellis, L. M.; Weihua, Z. Intracellular ATP Levels Are a Pivotal Determinant of Chemoresistance in Colon Cancer Cells. *Cancer Res.* **2012**, *72* (1), 304−314.
(65) Mo, R.; Jiang, T. Y.; DiSanto, R.; Tai, W. Y.; Gu, Z. ATP-Triggered Anticancer Drug Delivery. *Nat. Commun.* **2014**, *5*, 3364.
(66) Sigel, H.; Griesser, R. Nucleoside 5′-triphosphates: Self-Association, Acid-Base, and Metal Ion-Binding Properties in Solution. *Chem. Soc. Rev.* **2005**, *34* (10), 875−900.
(67) Ni, D. Z.; Ding, H.; Liu, S.; Yue, H.; Bao, Y. L.; Wang, Z. H.; Su, Z. G.; Wei, W.; Ma, G. H. Superior Intratumoral Penetration of Paclitaxel Nanodots Strengthens Tumor Restriction and Metastasis Prevention. *Small* **2015**, *11* (21), 2518−2526.
(68) Xu, X. D.; Wu, J.; Liu, Y. L.; Yu, M. Y.; Zhao, L. L.; Zhu, X.; Bhasin, S.; Li, Q.; Ha, E.; Shi, J. J.; Farokhzad, O. C. Ultra-pH-Responsive and Tumor-Penetrating Nanoplatform for Targeted siRNA Delivery with Robust Anti-Cancer Efficacy. *Angew. Chem., Int. Ed.* **2016**, *55* (25), 7091−7094.
(69) Liu, Z.; Sadler, P. J. Organoiridium Complexes: Anticancer Agents and Catalysts. *Acc. Chem. Res.* **2014**, *47* (4), 1174−1185.
(70) Graf, N.; Lippard, S. J. Redox Activation of Metal-Based Prodrugs as a Strategy for Drug Delivery. *Adv. Drug Delivery Rev.* **2012**, *64* (11), 993−1004.

DOI: 10.1021/acsami.7b03686
ACS Appl. Mater. Interfaces 2017, 9, 17757−17768